Supplementary Information for

2D-MoS_2 goes 3D: Transferring Optoelectronic Properties of 2D MoS_2 to a large-area thin film

Melanie Timpel[1,2,], Giovanni Ligorio[3], Amir Ghiami[1,4], Luca Gavioli[5], Emanuele Cavaliere[5], Andrea Chiappini[6], Francesca Rossi[7], Luca Pasquali[8,9,10], Fabian Gärisch[3], Emil J. W. List-Kratochvil[3,11], Petr Nozar[1], Alberto Quaranta[2], Roberto Verucchi[1], and Marco V. Nardi[1,*]*

[1]IMEM-CNR, Institute of Materials for Electronics and Magnetism, Trento unit c/o Fondazione Bruno Kessler, Via alla Cascata 56/C, Povo, Trento IT-38123, Italy.

[2]Department of Industrial Engineering, University of Trento, Via Sommarive 9, Trento IT-38123, Italy.

[3]Institut für Physik, Institut für Chemie & IRIS Adlershof, Humboldt-Universität zu Berlin, Zum Großen Windkanal 2 , 12489 Berlin, Germany.

[4]Department of Chemistry, Life Science and Environmental Sustainability - University of Parma, Parco Area delle Scienze 17/A, Parma IT-43124 Italy.

[5]Interdisciplinary Laboratories for Advanced Materials Physics (i-LAMP) and Dipartimento di Matematica e Fisica, Università Cattolica del Sacro Cuore, via dei Musei 41, Brescia IT-25121, Italy

[6]CNR-IFN, CSMFO Lab & FBK Photonics Unit, Via Alla Cascata 56/C, Trento IT-38123, Italy.

[7]IMEM-CNR, Institute of Materials for Electronics and Magnetism, Parco Area delle Scienze 37/A, Parma IT-43124, Italy.

[8]IOM-CNR Institute, Area Science Park, SS 14 Km, 163.5 – 34149 Basovizza, Trieste, Italy.

[9]University of Modena e Reggio Emilia, Engineering Department, "E. Ferrari", Via Vigolese 905 – 41125 Modena, Italy.

[10]Department of Physics, University of Johannesburg, PO Box 524, Auckland Park, 2006, South Africa.

[11]Helmholtz-Zentrum Berlin Für Materialien und Energie GmbH,
Hahn-Meitner-Platz 1, 14109, Berlin, Germany.

.

Email: *melanie.timpel@imem.cnr.it; marcovittorio.nardi@imem.cnr.it

Supplementary Notes

The main components of the IJD source[1-3] and the deposition geometry are depicted in Figure S1a. For MoS_2 thin film deposition via IJD, an ionized working gas (e.g., Ar^+) passes through a convergent-divergent De Laval nozzle[4] that creates an ultrafast (supersonic) gas flow in its widening part. This ionized gas jet enters a cylinder-shaped hollow cathode, in which the electrons of the ionized gas multiply and become electrostatically confined in an equipotential space. The fast oscillation of electrons within the hollow cathode leads to an avalanche/cascade ionization of the working gas, ultimately increasing the overall ionization density by orders of magnitude (hollow cathode effect).[5] Subsequently, the high-density electrons are discharged with a frequency $f \leq 300$ Hz (pulse length 100−300 ns) and are directed towards the grounded target

($|V| \leq 30$ kV, $I_{peak} \leq 6$ kA with a final pulse energy $E \leq 4$J). The highly energetic pulsed electron beam ablates a rotating MoS_2 target material and produces a plasma plume of ejected molecular-sized Mo_xS_y species that propagate with the working gas through the hollow cathode towards the rotating substrate. Finally, the Mo_xS_y species from the target condense as nm-sized clusters on the substrate, forming a MoS_2 thin film over a large area (e.g., covering 5-inch wafers or larger). The typical beam shape of a single IJD source (see Figure S1b) allows to uniformly coat 4-inch wafers, whereas larger areas can be coated using several IJD sources that are mounted in-line without the need of mechanical frame movements and/or beam scanning methods.

Supplementary Methods

In Figure S1c and d, the corresponding XPS core level analyses are shown, i.e., fitted Mo 3d + S 2s and S 2p core level spectra, respectively. The Mo $3d_{5/2}$ and $3d_{3/2}$ peaks stemming from Mo^{4+} species (gray-blue components in Figure S1c) are located at BE of 229.5 and 232.8 eV, respectively, and the S 2s peak (yellow component in Figure S1c) is found at 226.7 eV. The corresponding S $2p_{3/2}$ and $2p_{1/2}$ peaks stemming from S^{2-} in MoS_2 appear as a single component at BE of 162.3 eV (gray-blue component in Figure S1d). Additional S 2s and S 2p peaks are present (red components) at higher BEs (228.0 and 163.7 eV, respectively), suggesting that some sulfur atoms exhibit a different chemical environment (other than Mo−S) in the as-deposited thin film. This additional sulfur component can be attributed to S atoms that are not directly bound to Mo atoms such as in Mo−S−S species and elemental sulfur. Based on the spectra in Figure S1c and d, the atomic ratio of S/Mo is 2.45. The full width at half maximum (FWHM) of the fitted S 2p component is about 50% larger than those of the annealed MoS_2 (see Figure 1d in the main text), suggesting a defective atomic arrangement in the as-deposited MoS_2 nanoclusters. The XRD

spectrum in Figure S1e reveals no diffraction peaks, indicating an amorphous MoS_2 structure in the as-deposited sample.

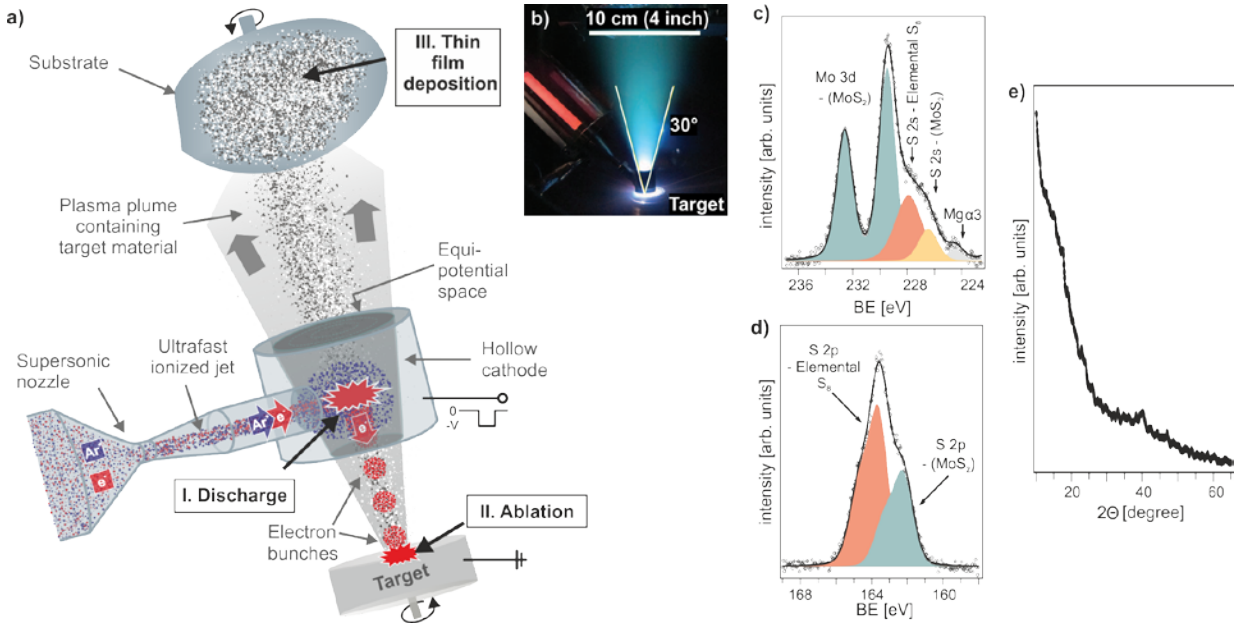

Supplementary Figure 1. Large-area MoS_2 thin film growth via ionized jet deposition (IJD): (a) schematic illustration of the main IJD components and typical deposition geometry; (b) typical beam shape produced by a standard 30°-aperture cathode; (c) fitted Mo 3d + S 2s and (d) S 2p core level spectra of as-deposited MoS_2 thin film; (e) corresponding XRD spectrum.

The morphology of the as-deposited and annealed MoS_2 thin film was analyzed by scanning electron microscopy (SEM) in a field-emission SUPRA40 Zeiss SEM equipped with a GEMINI FESEM detection column and using secondary electrons for imaging. The low-magnification SEM image of the as-deposited MoS_2 thin film in Figure S2a shows a homogenous and continuous morphology over the entire sample area, whereas the enlarged view in Figure S2b reveals a porous surface with a large (sub-µm) size distribution of the pores.

After annealing, homogenous regions are divided by cracks (see Figure S2c), which might be induced due to strain during annealing. The surface shown in the enlarged view in Figure S2d is representative for large sample areas of up to (120 × 120) μm^2. Its morphology appears less porous with respect to the as-deposited sample, i.e., larger pores have been eliminated by the annealing process. The low-magnification AFM image (20 µm × 20 µm) of the annealed MoS_2 thin film in Figure S2e confirms the morphology as observed by SEM.

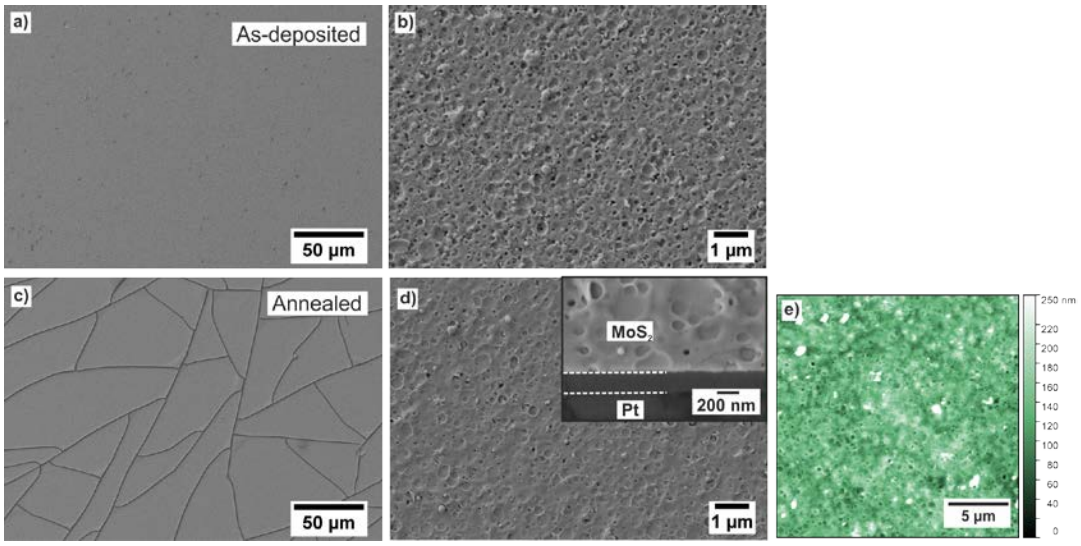

Supplementary Figure 2. (a) Low-magnification SEM image and (b) enlarged view of as-deposited MoS_2 thin film; (c) low-magnification SEM image and (d) enlarged view of annealed MoS_2 thin film (the inlet shows a cross-sectional SEM image for the determination of the thin film's thickness); (e) low-magnification AFM image (20 × 20 μm^2) of annealed MoS_2 thin film.

Figure S3a shows an optical micrograph, where different sample positions for PL measurements with λ = 532 nm (Figure S3b) are indicated. The PL lineshape (i.e., two sharp emission peaks) was found to be independent on the sample position, indicating optically active MoS_2 homogenously distributed in the annealed thin film. The PL spectrum acquired with another excitation wavelength of λ = 632 nm, i.e., corresponding to an energy slightly higher than the band gap of MoS_2, exhibits the same emission lineshape (see Figure S3c), which rules out any wavelength-induced effect on the PL spectrum. We rule out Raman scattering as the origin of the sharp features because changing the energy of the incident laser does not result in any corresponding shift in the emission energy.

Additional non-resonant Raman spectra (λ = 532 nm) of the annealed MoS_2 thin film were acquired in different sample positions (see Figure S3d). For the sake of comparison, the Raman spectra were aligned to the E^1_{2g} mode at ~383 cm^{-1}. It can be seen in Figure S3d that the value of frequency difference between the E^1_{2g} and A_{1g} modes slightly varies (19.5–23.1 cm^{-1}), which is consistent with the numbers of MoS_2 layers (L) observed in individual nanosheets (i.e., 1–4 L as evidenced by TEM, see Figure 3a in the main text).

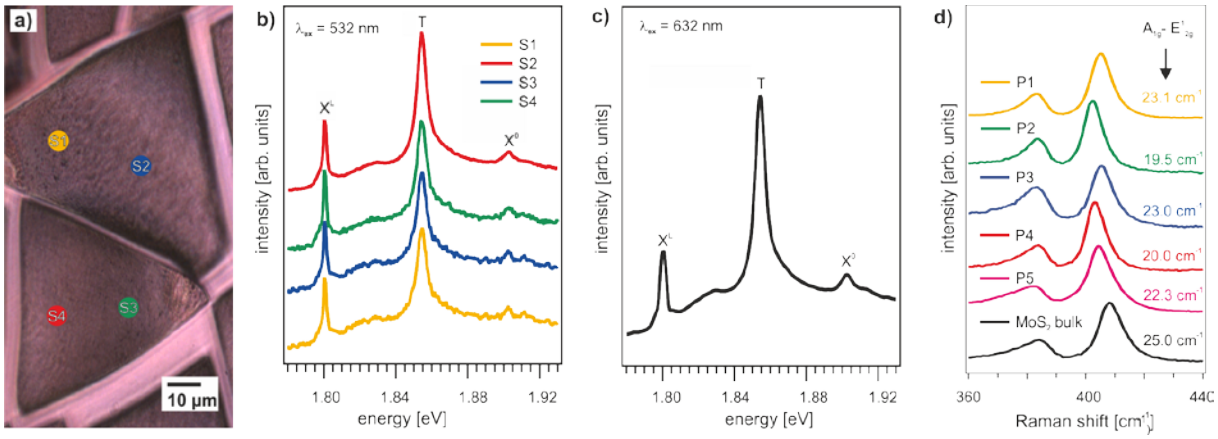

Supplementary Figure 3. (a) Optical micrograph showing different sample positions for PL measurements and (b) corresponding PL spectra (λ = 532 nm); (c) PL spectrum (λ = 632 nm) of annealed MoS_2 thin film; (d) non-resonant Raman (λ = 532 nm) spectra of different sample positions (spectra are aligned to the E^1_{2g} vibrations at 383.0 cm^{-1}), while MoS_2 bulk signal (black line) is shown for comparison.

Figure S4a displays an atomic-resolution STM image of crystalline 2D-MoS_2 nanosheets present in the annealed MoS_2 thin film. The corresponding FFT image in Figure S4b reveals a hexagonal lattice with a periodicity of (0.28 ± 0.06 nm), which is in good agreement to the S-to-S distance between the individual S-Mo-S layers (see Figure S4c).

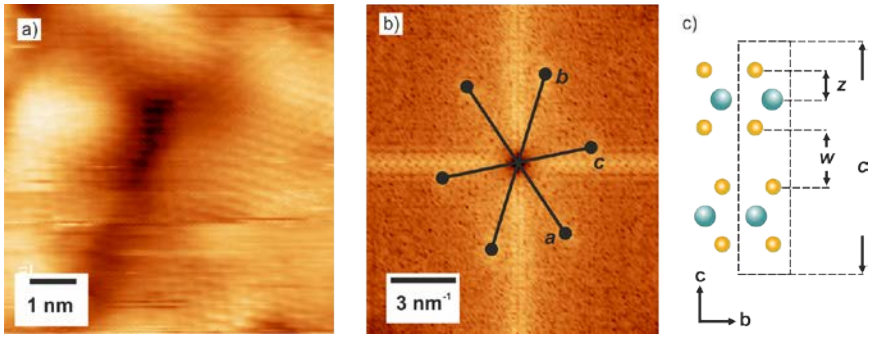

Supplementary Figure 4. (a) Atomic resolution STM image (V_{bias} = -1.1 V, 1.0 nA) and (b) corresponding FFT image of the MoS_2 nanosheets; c) top view of the 2H-MoS_2 crystal structure showing the Mo-to-S atomic layer distance of z =1.593 Å and the S-to-S distance between the individual S-Mo-S layers of w = 2.959 Å.[6]

In Figure S5 the electronic properties of as-deposited sample are reported. The work function was found to be Φ = 4.10 eV, whereas the onset of the VBM is not clearly defined. It is noteworthy that the electronic properties of the as-deposited thin film are reported for the sake of completeness, but they do not represent a well-defined crystalline MoS_2 sample (see results above).

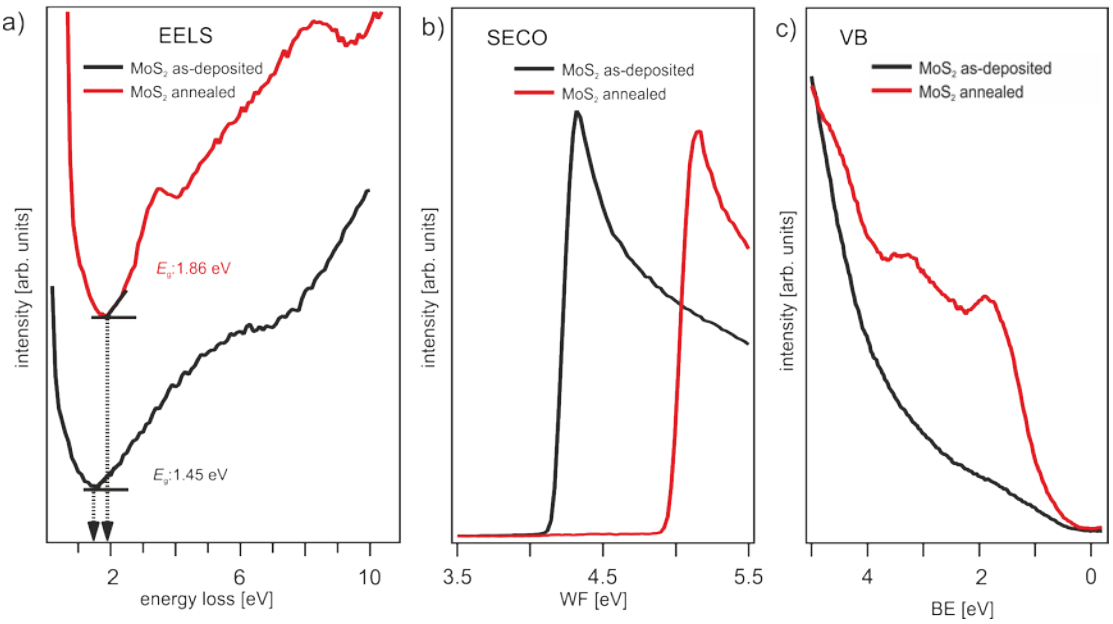

Supplementary Figure 5. (a) EELS, (b) SECO and (c) valence band (VB) region UPS spectra of as-deposited and annealed MoS_2 thin film.

Supplementary References

1 Lotti, R., Nozar, P., Taliani C. Device for Generating Plasma and for Directing an Flow of Electrons towards a Target, WO 2010/109297 A3 (2010).

2 Skocdopolova L., Device for Generating Plasma and Directing an Electron Beam towards a Target, WO 2013/186697 A2 (2013).

3 Skocdopolova, L. Un Apparato Ed Un Metodo per La Generazione Di Elettroni e Di Plasma Da Un Getto Di Gas. ITBO 20120320 A1 (2013).

4 Heinrich, P., Stoltenhoff, T., Richter, P., Kreye, H., Richter, H. Method and System for Cold Gas Spraying. US7143967; WO03041868; EP1390152; DE10126100 (2006).

5 Little, P. F., von Engel, A. The Hollow-Cathode Effect and the Theory of Glow Discharges. *Proc. R. Soc. A* **224**, 209–227(1954).

6 Dai, Z., Jin, W., Grady, M., Sadowski, J. T., Dadap, J. I., Jr, M. O., Pohl, K. Surface Structure of Bulk 2H-MoS2 (0001) and Exfoliated Suspended Monolayer MoS2: A Selected Area Low Energy Electron Diffraction Study. *Surf. Sci.* **660**, 16–21 (2017).